

# Nearest Neighbor Distances in SrTiO<sub>3</sub> and BaTiO<sub>3</sub> from the Projection Analysis of the Extended X-Ray Absorption Fine Structure

Alireza Bayat, Angelika Chassé, Reinhard Denecke, Stefan Förster, Paula Huth, Eva Maria Zollner, and Karl-Michael Schindler\*


An analysis of the extended X-ray absorption fine structure is developed, in which experimental modulations are projected onto calculated ones from backscattering at single neighboring atoms. From the extended X-ray absorption fine structures of single crystals of SrTiO<sub>3</sub> and BaTiO<sub>3</sub>, initial values for nearest neighbor distances are obtained. In addition, a preference for the element of the next nearest neighbor can be given.

## 1. Introduction

In X-ray absorption, the cross-section oscillates above the elemental absorption edge as the result of the interference of electron waves backscattered at neighboring atoms. The analysis of this extended X-ray absorption fine structure (EXAFS) is particularly useful for determining the geometric structures in systems with short-range order and limited long-range order.<sup>[1]</sup> Recent overviews about the theoretical description are given in previous studies.<sup>[2,3]</sup> The analysis proposed here aims at the very first step in structure determination, where an initial structural model for the subsequent structure refinement is created (Figure 1). Key parameters of such structural models are next neighbour distances to scattering atoms around the absorber atom. If no additional information from other investigations are available, distances are commonly derived from peak positions in Fourier transforms (FTs) of EXAFS modulations.

Dr. A. Bayat, Dr. A. Chassé, Dr. S. Förster, E. M. Zollner, Dr. K.-M. Schindler  
Institut für Physik  
Martin-Luther-Universität Halle-Wittenberg  
D-06099 Halle, Germany  
E-mail: karl-michael.schindler@physik.uni-halle.de

Prof. R. Denecke, P. Huth  
Wilhelm-Ostwald-Institut für Physikalische und Theoretische Chemie  
Universität Leipzig  
Linnéstraße 2, D-04103 Leipzig, Germany

 The ORCID identification number(s) for the author(s) of this article can be found under <https://doi.org/10.1002/pssb.201900621>.

© 2020 The Authors. Published by WILEY-VCH Verlag GmbH & Co. KGaA, Weinheim. This is an open access article under the terms of the Creative Commons Attribution-NonCommercial License, which permits use, distribution and reproduction in any medium, provided the original work is properly cited and is not used for commercial purposes.

DOI: 10.1002/pssb.201900621

FTs of EXAFS modulations neglect the dependence of the phase shift on the kinetic energy of the outgoing electron. As a result, peak positions in the FT are between 40 and 80 pm smaller than actual nearest neighbor distances, in particular if the spectrum has a limited energy range.<sup>[4–6]</sup> Heavy atoms present an additional feature: the phase shift varies strongly within a small energy range, which results in a modulation shape like a beating mode.<sup>[4]</sup>

Consequently, the FT of the modulation exhibits two peaks for one scatterer. By assuming the atomic number of a scatterer, these shortcomings can be corrected by transferring corrections from related systems<sup>[1]</sup> or applying phase and amplitude corrections to the modulation prior to the Fourier transformation.<sup>[7,8]</sup> Then, reasonable values for next neighbor distances in the initial structural model are obtained.

Rather than applying phase and amplitude corrections to experimental EXAFS modulations and project them onto trigonometric target functions with the Fourier transformation, phase and amplitude information can also be included in target functions using scattering calculations with one scatterer. Such an alternative approach has been developed for photoelectron diffraction (PED) modulations.<sup>[9,10]</sup> From the maxima of projection coefficients, initial values for next nearest neighbor distances were derived with an accuracy of  $\pm 10$  pm and below.<sup>[11]</sup>

In this publication, we develop a modified projection method for EXAFS modulations and apply it to experimental spectra of strontium titanate (SrTiO<sub>3</sub>) and barium titanate (BaTiO<sub>3</sub>) single crystals. Next neighbor distances will be derived from projection coefficients and compared with recent results from X-ray diffraction (XRD) investigations.<sup>[12–14]</sup> In addition, we will investigate whether the method can be extended to second and third nearest neighbors and elemental information about the scatterer can be obtained.

The cubic structure of SrTiO<sub>3</sub> has recently been determined by XRD.<sup>[12]</sup> The lattice vector of the unit cell has a length of 390.53 pm with a Ti–O distance of 195.27 pm and a Ti–Sr distance of 338.21 pm. The atomic numbers of O, Ti, and Sr (8, 22, and 38) cover more than a third of the periodic table. Due to the difference in scattering properties of the elements, at least the contributions from O and Sr might be distinguishable.

BaTiO<sub>3</sub> exhibits a ferroelectric to paraelectric phase transition at 395 K with a structural change from a tetragonal to a cubic unit cell. The structures of both phases have been determined

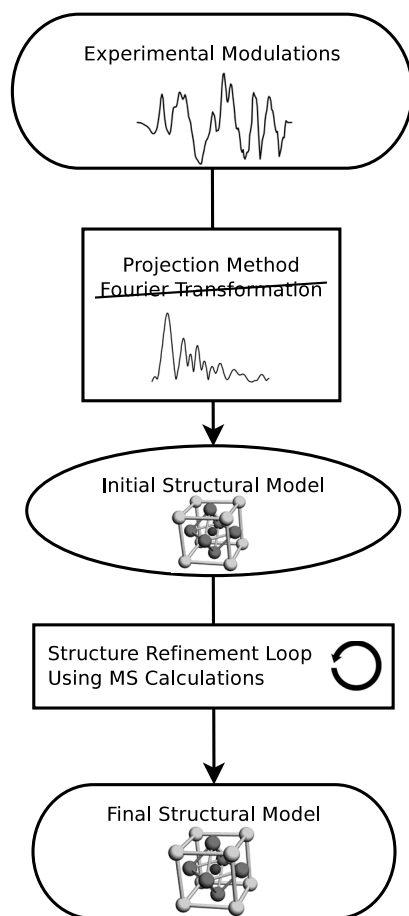


**Figure 1.** Structure determination based on EXAFS modulations.

using XRD.<sup>[13,14]</sup> The lattice constants of the tetragonal room-temperature phase are 399.25 and 403.73 pm, the one of the cubic phase at >413 K is 400.97 pm. The high precision interatomic distances serve as benchmark reference in the discussion of our results. Compared with SrTiO<sub>3</sub>, BaTiO<sub>3</sub> contains the heavier Ba atom with an atomic number of 56. The scattering properties of Ba differ more strongly from Ti and O than the ones of Sr. This might help to distinguish the contributions of elements. However, the Ba L<sub>3</sub>-edge is only 280 eV above the Ti K-edge, limits the energy range of EXAFS spectra, and may make the analysis of EXAFS modulations more difficult.

Finally, please note that we will neglect actual charge states of atoms and use the term atom instead of ion despite the dominantly ionic character of SrTiO<sub>3</sub> and BaTiO<sub>3</sub>.

## 2. Experimental Section

X-ray absorption spectra (XAS) were recorded in the ultrahigh vacuum (UHV) chamber of the HIKE beamline KMC-1 at the synchrotron light source BESSY II, Berlin. The photon energy range of the beamline from 2005 to 8000 eV included the Ti K-edge at 4.9 keV and the Ba L-edges at 5.2 and 5.6 keV. Its resolution  $\frac{\Delta E}{E}$  was 1000 at a photon energy of 4 keV.<sup>[15]</sup> Spectra were recorded as X-ray fluorescence yield (Bruker XFLASH R 4010

detector with a Be window) at 4.5 keV, covering the Ti K<sub>α<sub>1,2</sub></sub> and Ba L<sub>α<sub>1,2</sub></sub> X-ray emission lines.

Commercial single crystals of BaTiO<sub>3</sub> and SrTiO<sub>3</sub> (MaTeck) with polished (100) surfaces were cleaned by rinsing with deionized water in air before loading them into the vacuum chamber. For sufficient conductivity, the SrTiO<sub>3</sub> sample had been doped with 0.5% atomic weight of Nb. The pristine BaTiO<sub>3</sub> sample was found to be conducting enough, presumably due to doping by oxygen vacancies. For desorbing adsorbates, the samples were heated in vacuum at 330 K. Elemental composition and cleanliness were checked with high kinetic energy X-ray photoelectron spectroscopy (XPS). Overview spectra at a photon energy of 2503 eV using a dedicated high-energy hemispherical analyzer (Scienta R4000)<sup>[16]</sup> showed photoemission and Auger emission lines of all respective elements. Surface contaminants containing carbon in the range of a monolayer were also detected.

The experimental X-ray absorption data were analyzed using the software packages DEMETER<sup>[17,18]</sup> and IFEFFIT.<sup>[19,20]</sup> The analysis included background subtraction, normalization to the height of the step edge, determination of the step edge energy and I<sub>0</sub>, and k<sup>2</sup>-weighting.

## 3. Projection Method

In this method, a set of calculated EXAFS modulations is created based on the atomic numbers of absorber and scatterer atoms. Spherical wave fronts and all phase shifts along the scattering paths are considered by means of FEFF8-lite.<sup>[21]</sup> For all distances, the calculated modulation results from the single scattering path from the absorber atom to the neighboring atom and back to the absorber atom. For small distances, the neighbor–emitter–neighbor triple scattering path (rattle mode) makes a significant contribution to the calculated modulation and has been included. Multiple scattering paths, which include other neighboring atoms, are long and their resultant contribution is small enough to be neglected. The calculated modulations form the basis set of functions for the projection of experimental modulations.

The projection method is similar to the FT, where an experimental modulation is projected onto a set of orthonormal trigonometric functions. Because the calculated modulations have no imaginary part, projection coefficients are real numbers and slightly easier to interpret than complex Fourier coefficients. In the following, we derive all details of the projection method for EXAFS modulations.

The projection coefficient  $c(r_i)$  is calculated from experimental modulation  $\chi_{\text{expt}}$  and calculated modulation  $\chi_{\text{calc}}$  with the scatterer at absorber–scatterer distance  $r_i$  as follows

$$c(r_i) = \int_0^\infty \chi_{\text{expt}}(k) \cdot \chi_{\text{calc}}(k, r_i) dk \quad (1)$$

For now, the projection coefficient is a 1D function of the emitter–scatterer distance  $r_i$  with other parameters of the calculations (e.g., Debye–Waller factors) kept constant. In a later stage, such parameters can also be explored using multidimensional projection coefficients.

A typical experiment is based on measurements at discrete values in  $k_j$  derived from the kinetic energies of outgoing electrons. The experiment also sets an upper limit in  $k$  in

Equation (1). With a constant step width  $\Delta k$ , the integral in Equation (1) is approximated by a sum

$$c(r_i) = \sum_j \chi_{\text{expt}}(k_j) \cdot \chi_{\text{calc}}(k_j, r_i) \cdot \Delta k \quad (2)$$

In the PED version, the coefficients have been multiplied with  $r_i$  to prevent unreasonable high coefficients for low values of  $r_i$ .<sup>[9]</sup> With EXAFS modulations, we simply set a suitable lower limit in  $r_i$  at 1 Å and avoid the modification by the multiplication.

The coefficients of the original projection method do not correspond to the number of scattering atoms.<sup>[9]</sup> Here, we derive a normalization with a factor  $n(r_i)$  from the following idea: Let us assume that the experimental modulation consists of modulations resulting from a number of atoms all at the same distance. Then, the coefficient  $c(r_i)$  needs to be divided by the projection of the calculated modulation function onto itself, in other words, the normalization factor  $n(r_i)$  is defined as

$$n(r_i) = \sum_j \chi_{\text{calc}}(k_j, r_i) \cdot \chi_{\text{calc}}(k_j, r_i) \cdot \Delta k \quad (3)$$

and we define a normalized coefficient  $c_{\text{norm}}$  as

$$c_{\text{norm}}(r_i) = \frac{c(r_i)}{n(r_i)} = \frac{\sum_j \chi_{\text{expt}}(k_j) \cdot \chi_{\text{calc}}(k_j, r_i)}{\sum_j \chi_{\text{calc}}(k_j, r_i) \cdot \chi_{\text{calc}}(k_j, r_i)} \quad (4)$$

Please note that the fraction has been reduced by the step width  $\Delta k$ , which is correct as long as  $\Delta k$  is constant and identical in experiment and calculations. Raw and normalized projection coefficients  $c(r_i)$  and  $c_{\text{norm}}(r_i)$  are real numbers and large positive values indicate positions of neighboring scatterers. The oscillatory character of modulations can lead to an antiphase relation between experimental and calculated modulations resulting in negative projection coefficients  $c(r_i)$  and  $c_{\text{norm}}(r_i)$ . Because the coefficients are intended to indicate the presence of a scatterer, negative values have no physical meaning and are preferably replaced by zero or values close to zero. Taking the absolute of the negative coefficients is also not appropriate because this reverts the phase information required for ruling out these distances. In the original version for PED, negative values have been suppressed by inserting the projection coefficients  $c(r_i)$  in the exponential function.<sup>[9]</sup> In addition to the suppression of negative coefficients, the exponential function emphasizes large positive values. Together with the multiplication by  $r_i$ , the coefficients  $C(r_i)$  lose any direct correspondence to the coordination number of the emitter atom.

Our new approach for the transformation is based on the idea to set negative values to zero and keep positive values unchanged. A smooth variant of this transformation, i.e., a transformation with a continuously differentiable as well as bijective transfer function, is the positive branch ( $y > 0$ ) of a hyperbola with the straight line  $y = x$  as asymptote for positive  $x$  and the  $x$ -axis as asymptote for negative  $x$ . The equation of such a hyperbola is

$$y^2 - xy = a^2 \quad (5)$$

The shape parameter  $a$  controls the intercept of the hyperbola with the  $y$ -axis.

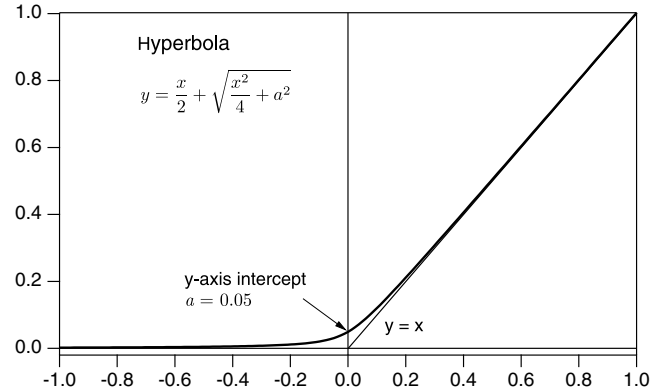


**Figure 2.** Projection coefficient transformation hyperbola according to Equation (6) with  $a = 0.05$ .

The transformation of  $c_{\text{norm}}(r_i)$  needs a rearranged Equation (5). The branch for  $y > 0$  is the positive part of the general solution of the quadratic equation

$$y = \frac{x}{2} + \sqrt{\frac{x^2}{4} + a^2} \quad (6)$$

Tests with our data have revealed that  $a = 0.05$  yields reasonable values of the transformed projection coefficient. The corresponding transfer function is shown in **Figure 2**. For other systems, the tests on  $a$  will need to be repeated. With  $a = 0.05$ , the transformed coefficient  $c_{\text{trans}}(r_i)$  becomes

$$c_{\text{trans}}(r_i) = \frac{c_{\text{norm}}(r_i)}{2} + \sqrt{\frac{c_{\text{norm}}^2(r_i)}{4} + 0.05^2} \quad (7)$$

Nearest neighbor distances are directly derived from the maxima of the coefficient  $c_{\text{trans}}(r_i)$ . Applying this method to experimental data will explore the limits of this approach similar to the discussion for PED.<sup>[11]</sup>

The projection coefficient reflects the agreement between calculated and experimental modulations. Maximizing it as a function of structural and nonstructural parameters of the calculations corresponds to the conventional least squares regression during the final structure refinement loop. So far, we see no apparent advantage of the projection method regarding the final parameter values or the convergence of the loop, mainly because the same theoretical calculations are used. A practical test of the validity of this presumption might still be worthwhile.

The projection method can be implemented in many programming languages and systems. We choose IgorPro from Wavemetrics<sup>[22]</sup> due to its ease of use and its excellent numeric and graphic capabilities. However, the algorithm is simple enough for ports to other analysis packages and programming languages, for example, the Demeter/Larch combo.<sup>[18,23]</sup>

## 4. SrTiO<sub>3</sub>

### 4.1. EXAFS Modulations

**Figure 3** shows the experimental absorption spectrum at the Ti K-edge from a SrTiO<sub>3</sub> single crystal with a (100) surface at room

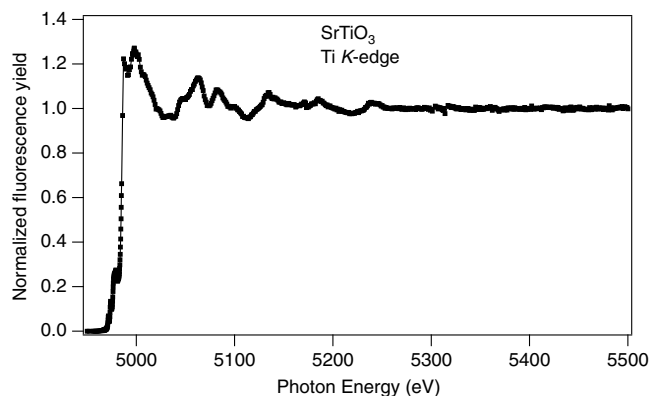


**Figure 3.** SrTiO<sub>3</sub>: experimental absorption spectrum at the Ti K-edge from fluorescence yield at 4.5 keV (Ti  $K_{\alpha_{1,2}}$ ) after background subtraction and normalization to step edge.

temperature. The upper limit of the spectrum was chosen as 5500 eV, above which modulations went below the noise level. From the raw spectrum, a linear background has been subtracted and the signal has been normalized to the height of the step edge. A step function is subtracted with the point of inflection at  $(4985.3 \pm 0.1)$  eV as position of the edge.

The energy range of the absorption spectrum translates to a maximum wave vector  $k$  of  $11.5 \text{ \AA}^{-1}$  for the outgoing electron. To compensate for the decrease in modulation amplitude at high  $k$ , the commonly used<sup>[24,25]</sup> weighting with  $k^2$  has been applied. It also suppresses the resonances in the near edge region, which are not well described with single scattering calculations. **Figure 4** shows the resulting modulations above the Ti K-edge of SrTiO<sub>3</sub>. Within the limits of experimental noise, the absorption spectrum and modulations correspond to published ones.<sup>[24–27]</sup>

#### 4.2. Projection Coefficients: Ti–O

**Figure 5a** shows the projection coefficients  $c_{\text{trans}}(r)$  of the Ti K-edge EXAFS modulations according to Equation (7) as a function of Ti–O distance  $r$ . The basis set of calculated modulation functions results from scattering calculations with an oxygen

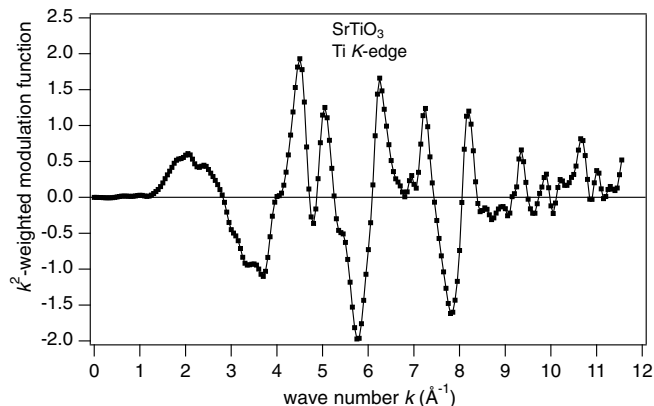


**Figure 4.** SrTiO<sub>3</sub>: experimental  $k^2$ -weighted EXAFS modulations above the Ti K-edge.

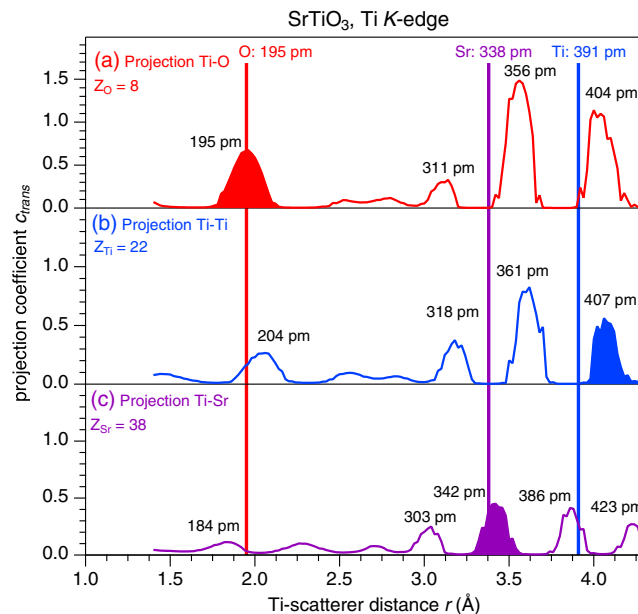


**Figure 5.** SrTiO<sub>3</sub>: projection coefficient  $c_{\text{trans}}$  of experimental Ti K-edge EXAFS modulations onto theoretical modulations with one scatterer as a function of distance: a) O scatterer, b) Ti scatterer, and c) Sr scatterer. Color bars and their labels indicate reference distances from XRD investigations.

scatterer at distances from 1.0 to 4.3 Å. The pronounced maximum at 195 pm is in excellent agreement with the Ti–O reference distance from XRD of 195.3 pm. The difference of 0.3 pm is far smaller than the expectation of 10 pm from the PED version.<sup>[11]</sup>

Further maxima of the projection coefficient show up at longer distances for 311, 356, and 404 pm. With the structure of SrTiO<sub>3</sub>, they result from scattering at other atoms and multiple scattering, which are not included in the calculations. Therefore, no structural information should be derived from these maxima.

#### 4.3. Projection Coefficients: Ti–Ti

The projection coefficients  $c_{\text{trans}}(r)$  according to Equation (7) with one neighboring Ti atom are shown in **Figure 5b**. Altogether, the coefficients are very similar to the ones for O, except for a shift of the peaks to larger distances by 3–9 pm and smaller values. In particular, the peak at 204 pm shows that the scattering properties of O and Ti are still too similar to distinguish them without any doubt.

From the three peaks at 318, 361, and 407 pm, only the one at 407 pm corresponds to a Ti atom. With a reference distance of 390.5 pm, the deviation is 16.5 pm, notably larger than with O. Presumably, 400 pm marks the limit in distance for significant assignments.

#### 4.4. Projection Coefficients: Ti–Sr

Finally, **Figure 5c** shows the projection coefficients  $c_{\text{trans}}(r)$  of the Ti K-edge EXAFS modulations as a function of Ti–Sr distance  $r$ .

The maxima are grouped into a set of three at low distances (184, 228, and 271 pm) and a set of four at high distances (303, 342, 386, and 423 pm). The peaks at low distances are small enough that they can be ruled out as Sr positions. Considering the structure of SrTiO<sub>3</sub>, we can assign the peak at 342 pm to Sr as second nearest neighbor. The value deviates only by 4 pm from its reference value and would therefore be very well suited as initial value for the final structure refinement loop. The reduced half width of this peak compared with the peak in the coefficients for O might result from the larger number of modulations for the larger distance.

The results from the analysis of the EXAFS modulations from a SrTiO<sub>3</sub> single crystal are summarized as follows: The next nearest O atoms are clearly resolved with very little deviation from the reference position (<1 pm). The magnitudes of the coefficients for Sr rule out the assignment of the peaks up to 270 pm to Sr. This is a gain compared with an analysis with an FT, where no indications about elements are obtained. After an assignment of the subsequent peaks to Sr and Ti, reasonable initial values for the distances of the second and third nearest neighbor are obtained without any further corrections. In cases, where the additional information is not available, two or three initial values are suggested for final structure refinement loops. It is then left to these loops, whether the ambiguity can be resolved on the basis of the EXAFS modulations alone or not.

## 5. BaTiO<sub>3</sub>

### 5.1. EXAFS Modulations

Figure 6 shows the experimental EXAFS modulation  $\chi^{(k)}$  above the Ti *K*-edge from the (100) surface of a BaTiO<sub>3</sub> single crystal. It has been obtained from the raw spectrum in the same way as the one for SrTiO<sub>3</sub>. Its range in *k* is limited to 8.1 Å<sup>-1</sup> due to the presence of the Ba *L*<sub>3</sub>-edge 280 eV above the Ti *K*-edge. Due to the overlap of the Ti *K*<sub>α</sub> and Ba *L*<sub>α</sub> fluorescence lines, the signal from the Ba *L*<sub>3</sub>-edge cannot be suppressed. As with SrTiO<sub>3</sub>, the commonly used weighting with *k*<sup>2</sup> has been applied to compensate the decrease in amplitude at higher *k*. The spectrum compares well with published data.<sup>[28,29]</sup>

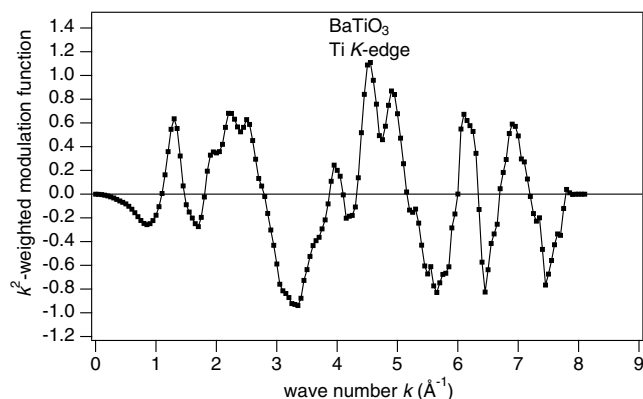


**Figure 6.** BaTiO<sub>3</sub>: experimental *k*<sup>2</sup>-weighted EXAFS modulations above the Ti *K*-edge from fluorescence yield at 4.5 keV (Ti *K*<sub>α<sub>1,2</sub></sub>) after background subtraction and normalization to step edge.

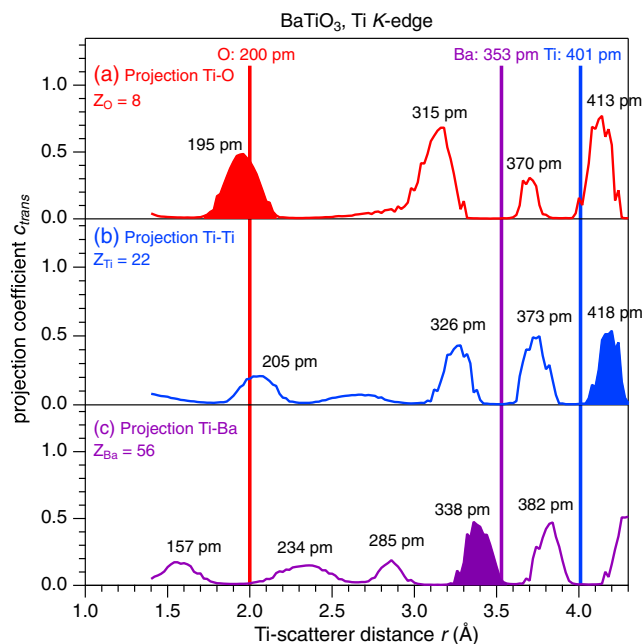
### 5.2. Projection Coefficients: Ti–O

Figure 7a shows the projection coefficients  $c_{\text{trans}}(r)$  of the Ti *K*-edge EXAFS modulations according to Equation (7) as function of Ti–O distance *r*. The first peak has a pronounced maximum at 195 pm, in excellent agreement with the Ti–O distances (182.9, 200.0, and 220.6 pm) from XRD investigations.<sup>[13,14]</sup> Its difference to the average at 200.0 pm is only 5 pm. Compared with SrTiO<sub>3</sub>, the peak is wider, but the broadening is too small to be taken as a significant hint to the short equatorial and long axial Ti–O distances.

Similar to SrTiO<sub>3</sub>, there are three peaks at 315, 370, and 413 pm. From knowing the structure, it is clear that they cannot stem from single scattering at O, but mimic scattering at Sr and Ti and multiple scattering.

### 5.3. Projection Coefficients: Ti–Ti

Figure 7b shows the projection coefficients  $c_{\text{trans}}(r)$  of the Ti *K*-edge EXAFS modulation according to Equation (7) as function of Ti–Ti distance *r*. As with SrTiO<sub>3</sub>, the coefficients are quite similar to the ones for O, again smaller and shifted to larger distances. Additional information for the decision between O or Ti as next nearest neighbor is required. The closest peak to the actual Ti position is at 418 pm, 17 pm off. We take this difference as an indication that 400 pm probably marks the limit of significant contributions.



**Figure 7.** BaTiO<sub>3</sub>: projection coefficient  $c_{\text{trans}}$  of experimental Ti *K*-edge EXAFS modulations onto theoretical modulations with one scatterer as a function of distance: a) O scatterer, b) Ti scatterer, and c) Ba scatterer. Color bars and their labels indicate reference distances from XRD investigations.

#### 5.4. Projection Coefficients: Ti–Ba

Figure 7c shows the projection coefficients  $c_{\text{trans}}(r)$  of the Ti K-edge EXAFS modulation as function of Ti–Ba distance  $r$ . Knowing the structure, the peaks at 157, 234, and 285 pm do not represent scattering at Ba atoms. Above 300 pm, there are peaks of equal heights at 338 and 382 pm. Ti–Ba reference distances are 348 and 358 pm, yielding an average of 353 pm. The differences of 15 and 29 pm give clear preference to assign the peak at 338 pm to Ti–Ba scattering paths.

## 6. Conclusions

The projection method as previously used in the structure determination with PED has been transferred and modified for the use with EXAFS modulations. The projection of the experimental modulation function onto calculated ones yields coefficients as a function of neighbor distances, which indicate the presence of scattering atoms. Tests with single crystals of SrTiO<sub>3</sub> and BaTiO<sub>3</sub> show that the projection method serves as a valid replacement of the Fourier transformation and yields initial values for next nearest neighbors with offsets below 5 pm. Relative peak heights rule out Sr as next nearest neighbor in both test systems. Although Ti atoms cannot completely be ruled out, O atoms are favored. Initial values for second and third nearest neighbors are obtained as sets of 2 or 3 values.

## Acknowledgements

This work was funded by the Deutsche Forschungsgemeinschaft (DFG, German Research Foundation)—project number 31047526—SFB 762 “Functionality of Oxide Interfaces,” projects A3 and A7. The authors acknowledge the mutual technical support within the SFB and the beamline staff at BESSY II, Berlin. Particular thanks go to R. Kulla for technical assistance, to D. Schindler for proof reading the mathematical parts, and to W. Widdra and members of his group for scientific discussions.

## Conflict of Interest

The authors declare no conflict of interest.

## Keywords

data analysis, extended X-ray absorption fine structures, projection method, structure determination

Received: September 30, 2019

Revised: February 24, 2020

Published online: March 18, 2020

- [1] P. A. Lee, P. H. Citrin, P. Eisenberger, B. M. Kincaid, *Rev. Mod. Phys.* **1981**, 53, 769.
- [2] J. J. Rehr, R. C. Albers, *Rev. Mod. Phys.* **2000**, 72, 621.
- [3] A. Kuzmin, J. Chaboy, *IUCrJ* **2014**, 1, 571.
- [4] B.-K. Teo, P. A. Lee, *J. Amer. Chem. Soc.* **1979**, 101, 2815.
- [5] J. Wong, *Mater. Sci. Eng.* **1986**, 80, 107.
- [6] K.-M. Schindler, P. Hofmann, V. Fritzsche, S. Bao, S. Kulkarni, A. M. Bradshaw, D. P. Woodruff, *Phys. Rev. Lett.* **1993**, 71, 2054.
- [7] J. B. A. D. van Zon, D. C. Koningsberger, H. F. J. van't Blik, D. E. Sayers, *J. Chem. Phys.* **1985**, 82, 5742.
- [8] D. C. Koningsberger, B. L. Mojet, G. E. van Dorssen, D. E. Ramaker, *Topics Catal.* **2000**, 10, 143.
- [9] P. Hofmann, K.-M. Schindler, *Phys. Rev. B* **1993**, 47, 13941.
- [10] P. Hofmann, K.-M. Schindler, S. Bao, A. M. Bradshaw, D. P. Woodruff, *Nature* **1994**, 368, 131.
- [11] D. P. Woodruff, P. Baumgärtel, J. T. Hoeft, M. Kittel, M. Polcik, *J. Phys.: Condens. Matter* **2001**, 13, 10625.
- [12] M. Schmidbauer, A. Kwasniewski, J. Schwarzkopf, *Acta Crystallogr. B* **2012**, 68, 8.
- [13] G. H. Kwei, A. C. Lawson, S. J. L. Billinge, S.-W. Cheong, *J. Phys. Chem.* **1993**, 97, 2368.
- [14] T. Nakatani, A. Yoshiasa, A. Nakatsuka, T. Hiratoko, T. Mashimo, M. Okube, S. Sasaki, *Acta Crystallogr. B* **2016**, 72, 151.
- [15] F. Schaefer, M. Mertin, M. Gorgoi, *Rev. Sci. Instrum.* **2007**, 78, 123102.
- [16] M. Gorgoi, S. Svensson, F. Schaefer, G. Ohrwall, M. Mertin, P. Bressler, O. Karis, H. Siegbahn, A. Sandell, H. Rensmo, W. Doherty, C. Jung, W. Braun, W. Eberhardt, *Nucl. Instrum. Methods Phys. Res. A* **2009**, 601, 48.
- [17] B. Ravel, M. Newville, *J. Synchrotron Rad.* **2005**, 12, 537.
- [18] Demeter, <https://bruceravel.github.io/demeter/> (accessed: December 2019).
- [19] M. Newville, *J. Synchrotron Rad.* **2001**, 8, 96.
- [20] IFEFFIT, <https://cars9.uchicago.edu/ifeffit/> (accessed: December 2019).
- [21] A. L. Ankudinov, B. Ravel, J. J. Rehr, S. D. Conradson, *Phys. Rev. B* **1998**, 58, 7565.
- [22] IgorPro, <https://www.wavemetrics.com> (accessed: December 2019).
- [23] Larch, <https://xraypy.github.io/xraylarch/> (accessed: December 2019).
- [24] A. Kuzmin, R. A. Evarestov, *J. Phys.: Condens. Matter* **2009**, 21, 055401.
- [25] A. Anspoks, J. Timoshenko, D. Bocharov, J. Purans, F. Rocca, A. Sarakovskis, V. Trepakov, A. Dejneka, M. Itoh, *Ferroelectrics* **2015**, 485, 42.
- [26] M. Fischer, A. Lahmar, M. Maglione, A. San Miguel, J. P. Itie, A. Polian, F. Baudelet, *Phys. Rev. B* **1994**, 49, 12451.
- [27] O. Kamishima, Y. Nishihata, H. Maeda, T. Ishii, A. Sawada, H. Terauchi, *Physica B* **1995**, 208–209, 303.
- [28] B. Ravel, E. A. Stern, R. I. Vedrinskii, V. Kraizman, *Ferroelectrics* **1998**, 206–207, 407.
- [29] A. I. Frenkel, M. H. Frey, D. A. Payne, *J. Synchrotron Rad.* **1999**, 6, 515.